Virtual element method for modeling the deformation of multiphase composites

N. Sukumar[a,*], John E. Bolander[a]

[a]*Department of Civil and Environmental Engineering, University of California, Davis, CA 95616, USA*

Abstract

In this paper, we study applications of the virtual element method (VEM) for simulating the deformation of multiphase composites. The VEM is a Galerkin approach that is applicable to meshes that consist of arbitrarily-shaped polygonal and polyhedral (simple and nonsimple) elements. In the VEM, the basis functions are defined as the solution of a local elliptic partial differential equation, and are never explicitly computed in the implementation of the method. The stiffness matrix of each element is built by using the elliptic projection operator of the internal virtual work (bilinear form) and it consists of two terms: a consistency term that is exactly computed (linear patch test is satisfied) and a correction term (ensures stability) that is orthogonal to affine displacement fields and has the right scaling. The VEM simplifies mesh generation for a multiphase composite: a stiff inclusion can be modeled using a single polygonal or polyhedral element. Attributes of the virtual element approach are highlighted through comparisons with Voronoi-cell lattice models, which provide discrete representations of material structure. The comparisons involve a suite of two-dimensional linear elastic problems: patch test, axisymmetric circular inclusion problem, and the deformation of a three-phase composite. The simulations demonstrate the accuracy and flexibility of the virtual element method.

Keywords: VEM, lattice models, Voronoi meshes, concrete composites, irregular-shaped inclusions

1. Introduction

Opportunities exist for designing multiphase materials with improved composite properties [1]. In many cases, these materials consist of one or more dispersed particulate (or fibrous) phases within a binding phase. Along with the properties of the individual phases, typically the behavior of the phase interfaces has primary influences on the composite properties, notably those related to fracture and mass transport. Concrete, which consists of aggregate inclusions embedded in a cement-based matrix, is a prime example of a multiphase particulate material that benefits from mesoscale analysis and design.

Even though continuum approaches, including the finite element method, have been used for mesoscale modeling of concrete materials, various discrete modeling approaches have also received much interest. Particle-based lattice models are advantageous in the simple and natural way cracks and other forms of displacement discontinuity are represented [2, 3], largely avoiding the stress-locking phenomenon associated with ordinary continuum representations of fracture. Such lattice models

permit deformation and fracture of inclusions (heterogeneities) to be efficiently represented and captured in simulations but they cannot in general exactly represent homogeneous deformation states (elastic homogeneity) for arbitrary Poisson's ratio ν [4]. In contrast, finite elements satisfy the patch test but the need for high-quality meshes for heterogeneous microstructures and the computational costs that are incurred limit the number of inclusions that can be explicitly modeled.

In this paper, we demonstrate the flexibility and capabilities that the virtual element method (VEM) [5] affords to model the deformation of multiphase composites, such as cement-based materials that contain aggregate inclusions. Some of the previous contributions in the modeling of the concrete mesostructure using the VEM are due to Benedetto et al. [6] and Rivarola et al. [7, 8]. We compare the performance of the VEM against a Voronoi-cell lattice model (VCLM) based on the rigid-body-spring concept of Kawai [9, 10]. Our emphasis in this paper is to promote VEM as a methodology that has the desirable attributes of such lattice models as well as the FEM to model multiphase materials (e.g., concrete composites).

The virtual element element (VEM) [5] is a stabilized high-order Galerkin discretizations on polygonal and polyhedral meshes to solve boundary-value problems. It provides a variational framework for the first order mimetic finite-difference scheme [11], and is a gen-

---
[*]Corresponding author
  Email addresses: nsukumar@ucdavis.edu (N. Sukumar), jebolander@ucdavis.edu (John E. Bolander)

eralization of hourglass finite elements [12] to polytopal meshes [13]. In the VEM, the basis functions are defined as the solution of a local elliptic partial differential equation, and are never explicitly computed (ergo the name *virtual*) in the implementation of the method. Over each element E in the mesh, the trial and test functions belong to the local discretization (virtual) space that consist of polynomials of order less than or equal to k (k is the order of the element) and in addition nonpolynomial functions. Since the virtual basis functions are unknown in each element, the VEM uses their elliptic polynomial projections to build the bilinear form (stiffness matrix) and continuous linear functional (body force term) of the variational formulation. Such projections are computable from the degrees of freedom within each element. The bilinear form on E consists of two parts: the consistency term that approximates the stiffness matrix on a given polynomial space and the correction term that ensures stability. Essential boundary conditions in the VEM are imposed as in the FEM, and element-level assembly procedures are used to form the global stiffness matrix and force vector.

A notable advantage of the VEM is that computations can be done over meshes with arbitrarily-shaped convex and nonconvex (simple and nonsimple) elements without needing to compute the shape functions (generalized barycentric coordinates [14]) on such elements. In particular, *hanging nodes* on nonmatching (quadtree or weakly convex elements) meshes lead to conforming approximations. This facilitates modeling bimaterial interfaces, such as those that arise between polygonal inclusions and the matrix in cement-based composites, and also simplifies the imposition of contact conditions along interfaces [15, 16]. Furthermore, mesh generation is simplified: an irregular-shaped stiff inclusion can be modeled using a single *polygonal virtual element* [17]. Many of these and other positive attributes of the VEM have been emphasized and demonstrated in the virtual element literature, initially for low- and high-order formulations for scalar elliptic problems [18–22] and more recently for linear and nonlinear problems in the deformation of solid continua [15, 16, 23–30].

In recent studies, the versatility of the VEM in composites modeling (multiphases, unit cell homogenization, and multiscale computations) has been shown [7, 8, 31, 32]. In this paper, we provide comparisons of the VEM versus Voronoi-cell lattice models for modeling the elastic deformation of two-dimensional multiphase composites, which serve as a basis for modeling fracture in future work. The comparisons highlight attributes of the VEM, including its accuracy and flexibility in discretizing multiphase materials.
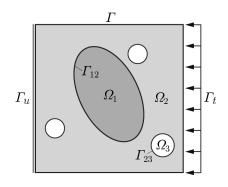

Figure 1: Elastostatic model problem for a three-phase composite.

2. Elastostatic Model for Multiphase Materials: Strong and Weak Formulations

Consider a linear elastic solid that occupies the domain $\Omega \subset \mathbb{R}^2$, with boundary $\Gamma = \partial\Omega$. The solid is composed of m isotropic, linearly elastic homogeneous materials, and the domain of each material is Ω_i, such that $\Omega = \overline{\Omega_1 \cup \Omega_2 \cup \ldots \cup \Omega_m}$. The boundary that defines the material interface between Ω_i and Ω_j is denoted by Γ_{ij}. The material interface is assumed to be perfectly bonded. The external boundary $\Gamma = \overline{\Gamma_u \cup \Gamma_t}$, with $\Gamma_u \cap \Gamma_t = \emptyset$. The boundary subsets Γ_u and Γ_t are where displacements and tractions are imposed, respectively. A schematic of the model problem for a three-phase composite is shown in Fig. 1.

In the absence of body forces, the governing equations of the elastostatic boundary-value problem are:

$$\nabla \cdot \boldsymbol{\sigma} = 0 \quad \text{in } \Omega, \tag{1a}$$

$$\boldsymbol{\sigma} = \mathbb{C}_i : \boldsymbol{\varepsilon} \quad \text{in } \Omega_i, \tag{1b}$$

$$\boldsymbol{\varepsilon} = \nabla_s \boldsymbol{u} \quad \text{in } \Omega, \tag{1c}$$

where $\boldsymbol{u}$ is the displacement field, ∇_s is the symmetric gradient operator, $\boldsymbol{\varepsilon}$ is the small-strain tensor, $\boldsymbol{\sigma}$ is the Cauchy stress tensor, and $\mathbb{C}_i$ is the material moduli tensor for a homogeneous, linear elastic isotropic material in the domain Ω_i ($i = 1, 2, \ldots, m$). The essential boundary conditions, traction boundary conditions, and interface conditions are:

$$\boldsymbol{u} = \bar{\boldsymbol{u}} \quad \text{on } \Gamma_u, \tag{2a}$$

$$\boldsymbol{n} \cdot \boldsymbol{\sigma} = \bar{\boldsymbol{t}} \quad \text{on } \Gamma_t, \tag{2b}$$

$$[[\boldsymbol{u}]] = \boldsymbol{0} \quad \text{on } \Gamma_{ij}, \tag{2c}$$

$$[[\boldsymbol{n} \cdot \boldsymbol{\sigma}]] = \boldsymbol{0} \quad \text{on } \Gamma_{ij}, \tag{2d}$$

where $\boldsymbol{n}$ is the unit vector that is normal to the indicated boundary and $[[\cdot]]$ is the jump operator that represents the jump in its argument across the interface.

The presence of a material (weak) discontinuity is met in the standard finite element method and also in the virtual element method via meshing the domain and its

internal and external boundaries so that Γ_{ij} is the union of element edges in the FE mesh. The additional advantage in the VEM is that this condition is retained even if nodal conformity is not met on an edge that is shared by two elements (*hanging nodes* are allowed). However, unlike use of polygonal finite elements that require shape functions over weakly convex polygons (quadtree meshes) [33], this is achieved in the VEM without the need to form the shape functions.

Let $\mathbb{U}_i$ ($i = 1, 2$) denote the affine subspace of functions in the Sobolev space $H^1(\Omega)$ whose trace on Γ_u is equal to $\bar{u}_i$ and whose normal derivative on Γ_{ij} is discontinuous. In addition, let $\mathbb{U}_0$ denote the linear subspace of functions in the Sobolev space $H^1(\Omega)$ that vanish on Γ_u and whose normal derivative on Γ_{ij} is discontinuous. The weak form of (1) and (2) is: find the trial displacement field $\boldsymbol{u} \in \mathbb{U}_1 \times \mathbb{U}_2$ such that

$$a(\boldsymbol{u}, \boldsymbol{v}) = \ell(\boldsymbol{v}) \quad \forall \boldsymbol{v} \in \mathbb{U}_0 \times \mathbb{U}_0, \tag{3a}$$

where $\boldsymbol{v}$ is the test displacement field, and the internal virtual work (bilinear form) $a(\cdot, \cdot)$ and the linear functional $\ell(\cdot)$ are given by

$$a(\boldsymbol{u}, \boldsymbol{v}) := \int_\Omega \boldsymbol{\sigma}(\boldsymbol{u}) : \boldsymbol{\varepsilon}(\boldsymbol{v}) \, d\boldsymbol{x}, \quad \ell(\boldsymbol{v}) := \int_{\Gamma_t} \bar{\boldsymbol{t}} \cdot \boldsymbol{v} \, ds. \tag{3b}$$

3. Virtual Element Method for Plane Elasticity

The formulation and implementation of the lowest-order virtual element method for 2D and 3D solid continua is well-documented [19, 24, 25, 28, 30]. We follow the exposition in Sukumar and Tupek [30] to present the main elements of VEM for 2D solid continua.

3.1. Decomposition of the domain

Let $\Omega \subset \mathbb{R}^2$ be the problem domain and $\mathcal{T}^h$ a decomposition of Ω into nonoverlapping polygons (simple or nonsimple). The number of nodes in $\mathcal{T}^h$ is N. We refer to $E \in \mathcal{T}^h$ as an *element*. The vertices of E are denoted by v_i, and the coordinate of vertex v_i by $\boldsymbol{x}_i := (x_i, y_i)$. The diameter, centroid (barycenter) and area of E are denoted by h_E. $\boldsymbol{x}_E$ and $|E|$, respectively. A polygon E has N_E vertices and N_E edges, with the edges denoted by e_i ($i = 1, 2, \ldots, N_E$). For the convergence proofs, restrictions are placed on the shape-regularity of the elements [5].

3.2. Polynomial spaces and virtual element space

Let $\mathbb{P}_k(E)$ be the function space on E that consists of all polynomials of order less than or equal to k. By convention, $\mathbb{P}_{-1} = \{0\}$. The dimension of $\mathbb{P}_k(E)$ is denoted by $\dim \mathbb{P}_k(E)$, and $\dim \mathbb{P}_k(E) = (k + 1)(k + 2)/2$ in two dimensions. The set consisting of the scaled monomials

of order less than or equal to k on E is defined as $\mathcal{M}_k(E)$. In this paper, we use the first-order VEM ($k = 1$). In two dimensions,

$$\mathbb{P}_1(E) = \{1, \, x, \, y\}, \quad \mathcal{M}_1(E) = \left\{1, \, \frac{x - x_E}{h_E}, \frac{y - y_E}{h_E}\right\}$$

are the first-order (polynomial and scaled monomial, respectively) basis sets. All elements in $\mathcal{M}_1(E)$ are of $O(1)$.

Let $\boldsymbol{P}_1(E) = [\mathbb{P}_1(E)]^2$ be the polynomial basis for a vector field in $\mathbb{R}^2$. For planar linear elasticity, there are three rigid-body (zero-energy) modes. Let

$$\xi := \frac{x - x_E}{h_E}, \quad \eta := \frac{y - y_E}{h_E}. \tag{4}$$

For 2D solid continua, we define $\widehat{\boldsymbol{M}}(E) := \boldsymbol{M}_1(E)$ as the scaled monomial first-order vectorial basis set:

$$\widehat{\boldsymbol{M}}(E) = \left[\begin{Bmatrix} 1 \\ 0 \end{Bmatrix}, \begin{Bmatrix} 0 \\ 1 \end{Bmatrix}, \begin{Bmatrix} -\eta \\ \xi \end{Bmatrix}, \begin{Bmatrix} \eta \\ \xi \end{Bmatrix}, \begin{Bmatrix} \xi \\ 0 \end{Bmatrix}, \begin{Bmatrix} 0 \\ \eta \end{Bmatrix}\right], \tag{5}$$

where the first three vectorial bases in (5) contain the rigid-body modes.

Let $V(E)$ denote the first-order virtual element space on element E. The virtual element space for 2D solid continua is [23]:

$$V(E) = \left\{\boldsymbol{v}^h : \boldsymbol{v}^h \in [H^1(E)]^2, \, \Delta \boldsymbol{v}^h = \boldsymbol{0},\right.$$
$$\left. \boldsymbol{v}^h|_e \in \boldsymbol{P}_1(e) \, \forall e \in \partial E, \, \boldsymbol{v}^h|_{\partial E} \in [C^0]^2(\partial E)\right\},$$

where $\boldsymbol{v}^h$ is a piecewise continuous affine vector polynomial on the boundary of the polygon.

3.3. Computation of energy projection matrices

For linear elasticity, we take the values of $\boldsymbol{v}^h$ at the vertices of the polygon as its degrees of freedom (DOFs). Let $\{\phi_i\}_{i=1}^{N_E}$ be virtual canonical basis functions that satisfy the Lagrange interpolation property, $\phi_i(\boldsymbol{x}_j) = \delta_{ij}$. Define the vectorial basis function matrix:

$$\boldsymbol{\varphi} = \begin{bmatrix} \phi_1 & \ldots & \phi_{N_E} & 0 & \ldots & 0 \\ 0 & \ldots & 0 & \phi_1 & \ldots & \phi_{N_E} \end{bmatrix}$$
$$:= \begin{bmatrix} \boldsymbol{\varphi}_1 & \ldots & \boldsymbol{\varphi}_{N_E} & \boldsymbol{\varphi}_{N_E+1} & \ldots & \boldsymbol{\varphi}_{2N_E} \end{bmatrix}, \tag{6}$$

where $\boldsymbol{\varphi}_i = \{\phi_i \, 0\}^T$ and $\boldsymbol{\varphi}_{N_E+i} = \{0 \, \phi_i\}^T$ for $i = 1, \ldots, N_E$, are the $2N_E$ vectorial basis functions. The trial displacement field in E is:

$$\boldsymbol{v}^h(\boldsymbol{x}) = \sum_{i=1}^{2N_E} \boldsymbol{\varphi}_i(\boldsymbol{x}) v_i := \sum_{i=1}^{2N_E} \boldsymbol{\varphi}_i(\boldsymbol{x}) \mathtt{dof}_i(\boldsymbol{v}^h), \tag{7}$$

where v_i are scalar coefficients and $\mathtt{dof}_i(\cdot)$ extracts the i-th DOF of its argument.

Let $a_E^h(\cdot, \cdot)$ represent the discrete bilinear form of the countinuous operator in (3a). The variational problem

to determine the projector is determined via the energy orthogonality condition:

$$a_E^h(\boldsymbol{m}_\alpha, \boldsymbol{v}^h - \Pi^\varepsilon \boldsymbol{v}^h) = 0 \quad \forall \boldsymbol{m}_\alpha \in \widehat{\boldsymbol{M}}(E), \tag{8a}$$

which is supplemented by the condition:

$$P_0(\boldsymbol{m}_\alpha, \boldsymbol{v}^h - \Pi^\varepsilon \boldsymbol{v}^h) = 0 \quad (\alpha = 1, 2, 3), \tag{8b}$$

$$P_0(u, v) = \frac{1}{N_E} \sum_{j=1}^{N_E} \boldsymbol{u}(\boldsymbol{x}_j) \cdot \boldsymbol{v}(\boldsymbol{x}_j), \tag{8c}$$

where the projector $P_0(\cdot, \cdot)$ defines a discrete L^2 inner product on E. Note that for $\alpha = 1, 2, 3$, (8a) yields $0 = 0$.

On using (6), we define

$$\Pi^\varepsilon \boldsymbol{\varphi}_i = \sum_{\beta=1}^{6} \boldsymbol{m}_\beta \pi_\beta^i = \widehat{\boldsymbol{M}} \boldsymbol{\pi}^i \quad (i = 1, 2, \ldots, 2N_E) \tag{9}$$

as the projection of the i-th vectorial basis function onto the scaled monomial basis set, where π_β^i are unknown coefficients. On substituting $\boldsymbol{v}^h = \boldsymbol{\varphi}_i$ ($i = 1, 2, \ldots 2N_E$) in (8), using the divergence theorem on the right-hand side and linear momentum balance ($\nabla \cdot \boldsymbol{\sigma} = \boldsymbol{0}$), we obtain the linear system of equations:

$$\boldsymbol{G}\boldsymbol{\Pi} = \tilde{\boldsymbol{B}}, \quad \boldsymbol{\Pi} = \boldsymbol{G}^{-1}\tilde{\boldsymbol{B}}, \tag{10a}$$

$$\boldsymbol{G}_{\alpha\beta} = \begin{cases} \frac{1}{N_E} \sum_{j=1}^{N_E} \boldsymbol{m}_\alpha(\boldsymbol{x}_j) \cdot \boldsymbol{m}_\beta(\boldsymbol{x}_j) & (\alpha = 1, 2, 3) \\ \boldsymbol{\sigma}(\boldsymbol{m}_\alpha) : \boldsymbol{\varepsilon}(\boldsymbol{m}_\beta) |E| & (\alpha = 4, 5, 6) \end{cases}, \tag{10b}$$

$$\tilde{\boldsymbol{B}}_{\alpha i} = \begin{cases} \frac{1}{N_E} \sum_{j=1}^{N_E} \boldsymbol{m}_\alpha(\boldsymbol{x}_j) \cdot \boldsymbol{\varphi}_i(\boldsymbol{x}_j) & (\alpha = 1, 2, 3) \\ \boldsymbol{\sigma}(\boldsymbol{m}_\alpha) : \sum_{j=1}^{N_E} \int_{e_j} \boldsymbol{\varphi}_i \otimes \boldsymbol{n}_j \, ds & (\alpha = 4, 5, 6) \end{cases}, \tag{10c}$$

where $\boldsymbol{\Pi} = [\boldsymbol{\pi}^1, \boldsymbol{\pi}^2, \ldots, \boldsymbol{\pi}^{2N_E}]$ is the matrix representation of the projection of the canonical basis functions in the scaled monomial basis set. The boundary integral in (10c) can be exactly computed using a two-point Gauss-Lobatto quadrature scheme.

Using the decomposition $\boldsymbol{\varphi}_i = \Pi^\varepsilon \boldsymbol{\varphi}_i + (1 - \Pi^\varepsilon)\boldsymbol{\varphi}_i$ in the bilinear form and the orthogonality condition (8a), the stiffness matrix can be expressed as:

$$\boldsymbol{K}_E = \boldsymbol{K}_E^c + \boldsymbol{K}_E^s,$$
$$\boldsymbol{K}_E^c = \boldsymbol{\Pi}^T \tilde{\boldsymbol{G}} \boldsymbol{\Pi},$$
$$\boldsymbol{K}_E^s = (\boldsymbol{I} - \boldsymbol{D}\boldsymbol{\Pi})^T a_E^h(\boldsymbol{\varphi}, \boldsymbol{\varphi}) (\boldsymbol{I} - \boldsymbol{D}\boldsymbol{\Pi}),$$

and to ensure stability we approximate $a_E^h(\boldsymbol{\varphi}, \boldsymbol{\varphi})$ by a diagonal matrix $\boldsymbol{S}_E^d$ that scales as $\boldsymbol{K}_E^c$:

$$\boldsymbol{K}_E^s := (\boldsymbol{I} - \boldsymbol{D}\boldsymbol{\Pi}) \, \boldsymbol{S}_E^d \, (\boldsymbol{I} - \boldsymbol{D}\boldsymbol{\Pi}),$$

where $\boldsymbol{K}_E^c$ and $\boldsymbol{K}_E^s$ are the consistency and stabilization matrices, respectively, and $\tilde{\boldsymbol{G}}$ is the matrix $\boldsymbol{G}$ with its first three rows set to zero. In addition, $\boldsymbol{D}_{i\alpha} = \text{dof}_i(\boldsymbol{m}_\alpha)$ is the DOF-matrix and the i-th diagonal entry of $\boldsymbol{S}_E^d$ is chosen as $\max(\text{tr}(\boldsymbol{C})/3, (\boldsymbol{K}_E^c)_{ii})$ [22], where $\boldsymbol{C}$ is the isotropic linear elastic constitutive matrix.

3.4. Assembly and solution procedure

On the natural boundary Γ_t, the virtual element shape functions are identical to piecewise linear finite elements. So on using (3b), the element force vector $\boldsymbol{f}_E = \ell(\boldsymbol{\varphi})$ is computed. Having computed $\boldsymbol{K}_E$ for each element, we then perform standard finite element assembly procedures to form the global stiffness matrix $\boldsymbol{K}$ and the global force vector $\boldsymbol{f}$. On incorporating the essential boundary conditions, the linear system is solved to obtain the nodal displacement vector $\boldsymbol{d}$.
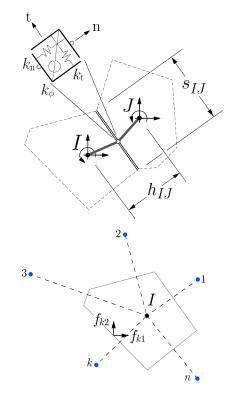
4. Voronoi-Cell Lattice Models

Figure 2: Voronoi-cell lattice element based on the rigid-body-spring concept (top); and spring-set force components for nodal stress calculation (bottom).

Particle-based lattice models share many features with classical lattice models, yet they differ in that each node is positioned within a geometric construct, or particle. In this case, the Voronoi diagram is used to partition the domain, such that each lattice node is associated with a Voronoi cell. For elasticity problems, the lattice element formulations are based on the rigid-body-spring concept of Kawai [9]. The Voronoi cells are assumed to be rigid and interconnected via zero-size spring sets located midway along the facets common to neighboring cells (Fig. 2). The stiffness matrices of these lattice elements are akin to those of ordinary frame elements and

4

assemble into the system stiffness matrix in the conventional manner. The spring sets contain components that are normal and tangential to the corresponding Voronoi facet. When these spring components have the same stiffness (i.e., $k_n = k_t$), the assembly of lattice elements is elastically homogeneous under uniform straining [10], albeit with $\nu = 0$.

The desired representation of both elastic constants (Young's modulus and Poisson's ratio) can be achieved, in a macroscopic sense, by appropriately setting the spring stiffness coefficients [34–36]. The assignment of spring coefficients depends on the type of loading. For the case of plane stress, and the type of random lattice considered herein, the coefficients can be determined according to [36]

$$\nu = \frac{1 - \alpha}{3 + \alpha}, \tag{11a}$$

$$E = E_0 \frac{2 + 2\alpha}{3 + \alpha}, \tag{11b}$$

where $\alpha = k_t/k_n$ and E_0 is the effective elastic modulus at the element level. Alternatively, Asahina et al. [37, 38] have developed a procedure (based on $k_n = k_t$) in which the Poisson effect is introduced iteratively using the concept of auxiliary stress. This provides both local and global representations of elastic behavior.

5. Numerical Examples

Numerical simulations are performed using the VEM and VCLM models on a suite of two-dimensional test problems. Within each example, the same Voronoi tessellation is used to define each model.

5.1. Patch test

The VEM and VCLM models are assessed on the displacement patch test. Two forms of VCLM are considered in this example: (a) global representation of elastic behavior according to (11a) and (11b); and (b) elastic behavior based on $k_n = k_t$ and the iterative introduction of the Poisson effect.

The meshes utilized for the patch test are shown in Fig. 3. On all meshes, including the mesh in Fig. 3c that contains a nonsimply-connected element, the VEM passes the patch test as indicated in Table 1. The performance of the VCLM depends on the aforementioned assignment of its spring coefficients. When using (11a) and (11b), such that $k_n \neq k_t$, relative errors are $O(10^{-2})$. This outcome has been viewed, with arguably some merit, as an effective means for representing the heterogeneity of concrete materials [34]. By setting $k_n = k_t$ and introducing the effect of Poisson's ratio using auxiliary stresses, however, the VCLM passes the patch test. For both VEM and VCLM ($k_n = k_t$), the errors in the stress

components are also found to be within machine precision. We point out that if $k_n = k_t$ is used in VCLM, but without the auxiliary stress modifications in the algorithm, then the displacement field matches the exact solution yet the computed stresses correspond to the case of $\nu = 0$.

Table 1: L^2 norm of the error in the displacement for the patch test.

| Model | Discretization | | |
	Fig. 3a	Fig. 3b	Fig. 3c
VEM	2×10^{-16}	4×10^{-16}	1×10^{-16}
VCLM ($k_n \neq k_t$)	4×10^{-02}	4×10^{-02}	–
VCLM ($k_n = k_t$)	3×10^{-16}	2×10^{-16}	–

5.2. Bimaterial subjected to axisymmetric plane strain

We consider a two-phase composite that occupies a circular region of radius b. The inclusion, Ω_1, is a disk of radius a and the matrix is defined by the region $\Omega_2 = \{r : a < r \leq b\}$. A radial displacement of magnitude b is imposed on $r = b$. Due to axisymmetry, the displacement field is: $\boldsymbol{u}(r, \theta) = u_r(r)\boldsymbol{e}_r$ in which $u_r(r)$ is a nonzero radial displacement field. A schematic illustration of the boundary-value problem is shown in Fig. 4, along with a Voronoi-cell discretization of the bimaterial domain that defines both the VEM and lattice models. This problem was first proposed in Sukumar et al. [39], and serves as a benchmark problem in computational solid mechanics [40]. The exact displacement field is [39]:

$$u_r(r) = \begin{cases} \left[\left(1 - \frac{b^2}{a^2}\right)\alpha + \frac{b^2}{a^2}\right]r & 0 \leq r \leq a \\ \left(r - \frac{b^2}{r}\right)\alpha + \frac{b^2}{r} & a < r \leq b \end{cases},$$

$$u_\theta = 0,$$

where

$$\alpha = \frac{(\lambda_1 + \mu_1 + \mu_2)\,b^2}{(\lambda_2 + \mu_2)\,a^2 + (\lambda_1 + \mu_1)\,(b^2 - a^2) + \mu_2 b^2},$$

and λ_1 and μ_1 and λ_2 and μ_2 are the Lamé parameters in Ω_1 and Ω_2, respectively.

This problem is solved for several values of the modular ratio $\eta = E_1/E_2$ with $a/b = 0.25$ and $\nu_1 = \nu_2 = 0.3$. Table 2 presents relative L^2 norm of the error in the displacement field for the VEM and VCLM models. For $\eta = 1$, the material is homogeneous, leading to uniform biaxial tension throughout the domain. Both methods simulate this condition with high precision.

Figure 5 plots major principal stress as a function of distance from the center of the inclusion. The exact solution for the stress components is:

$$\sigma_{rr}(r) = 2\mu_i\varepsilon_{rr}(r) + \lambda_i(\varepsilon_{rr}(r) + \varepsilon_{\theta\theta}(r)), \tag{12a}$$

$$\sigma_{\theta\theta}(r) = 2\mu_i\varepsilon_{\theta\theta}(r) + \lambda_i(\varepsilon_{rr}(r) + \varepsilon_{\theta\theta}(r)), \tag{12b}$$
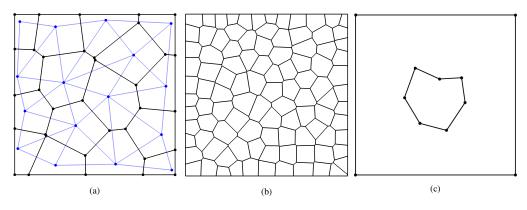
Figure 3: Displacement patch test for different discretization schemes. The displacement field $u(x, y) = 1 + x + y$, $v(x, y) = 2 - 3x - 4y$ is imposed on nodes (or generator points) that lie on (or adjacent to) the boundary of the square. (a) Coarse Voronoi cell discretization, indicating element connectivities defined by the Voronoi vertices and lattice element connectivities defined by the Voronoi generator points; (b) fine Voronoi cell discretization; and (c) single virtual element discretization of a square region containing an irregularly-shaped inclusion. The mesh in (c) consists of two virtual elements: the inner element is a nonconvex septagon and the outer element is a nonsimply-connected polygon with an inner boundary (seven nodes in clockwise orientation) and an outer boundary (four nodes in counter-clockwise orientation).

Table 2: Relative L^2 norm of the error in the displacement for the bi-material problem.

| Model | Modular ratio η | | |
	1	10	100
VEM	1.2×10^{-15}	1.5×10^{-3}	1.8×10^{-3}
VCLM	2.5×10^{-10}	2.7×10^{-3}	3.9×10^{-3}

where $\varepsilon_{rr}(r) = du_r(r)/dr$ and $\varepsilon_{\theta\theta}(r) = u_r(r)/r$; the subscript on the Lamé constants indicates the material subdomain.

For the lattice simulations, the volume-averaged stresses are computed at the lattice nodes via the relation [41]

$$
\begin{aligned}
\bar{\boldsymbol{\sigma}} &= \frac{1}{V} \int_C \boldsymbol{\sigma} \, d\boldsymbol{x} = \frac{1}{V} \int_C [\boldsymbol{I} \cdot \boldsymbol{\sigma} + \boldsymbol{x} \otimes (\nabla \cdot \boldsymbol{\sigma})] \, d\boldsymbol{x} \\
&= \frac{1}{V} \int_C (\boldsymbol{x} \otimes \boldsymbol{\sigma}^T) \cdot \nabla \, d\boldsymbol{x} = \frac{1}{V} \int_{\partial C} \boldsymbol{x} \otimes (\boldsymbol{n} \cdot \boldsymbol{\sigma}) \, dS \\
&= \frac{1}{V} \int_{\partial C} \boldsymbol{x} \otimes \boldsymbol{t} \, dS \approx \frac{1}{V} \sum_{k=1}^{n_f} \boldsymbol{x}_k \otimes \boldsymbol{f}_k,
\end{aligned}
\tag{13}
$$

where C is the Voronoi cell and ∂C is its boundary. The stress tensor is assumed to be divergence-free (no body forces are present) and $\boldsymbol{t}$ are the boundary tractions. In addition, $\boldsymbol{f}_k$ is a system of n_f external forces acting on the corresponding Voronoi cell having volume V; the forces act at locations $\boldsymbol{x}_k$ with respect to the cell node. Note that the stress tensor as defined in (13) is not symmetric, which is consistent with the behavior of a discrete lattice model as a micropolar (Cosserat) continuum [41].

The simulated stress profiles in the radial direction (Fig. 5, top) agree well with theory for the range of η values considered. For the VCLM model, the elements that span the Γ_{12} boundary are assigned the harmonic mean values of the properties of domains Ω_1 and Ω_2. Furthermore, the Voronoi generator points that define the boundary are positioned close to the boundary. These conditions improve the accuracy of the stress calculations near the boundary.

For cases of dispersed stiff inclusions, where the degree of modular mismatch is high, the stress field in the inclusions is approximately uniform. Such inclusions can be represented using a single VEM element, as shown in Fig. 4 (bottom). The radial stress value calculated for this single element, and plotted at $r/b = 0$ in Fig. 5 (bottom), has a relative error of 3.0×10^{-3}. For the region $r > a$, the radial stress values for the two cases (i.e., for the fully discretized and single-element representations of the inclusion) are essentially the same.

5.3. Three-phase composite

Capabilities of the VEM, and its correspondence to the VCLM, are further demonstrated through elastic analysis of a three-phase composite material. Figure 6a shows the planar discretization of a model porous concrete, in which disk-shaped aggregate inclusions are coated with a uniformly thick layer of hardened cement paste; the lightest shaded regions represent large-scale porosity between the paste layers. Compressive load is applied in the form of a uniform downward displacement of the uppermost vertices (or nodes), producing an average vertical strain of $\bar{\epsilon}_y$. The modular ratio of the inclusion and cement paste materials is $E_1/E_2 = 3$. Poisson's ratio is set as $\nu = 0.2$ for both phases, and plane stress conditions are assumed.

For the applied loading, Fig. 6 shows contours of minor principal stress, which highlight the nonuniform transfer of load through the material. Stress risers occur
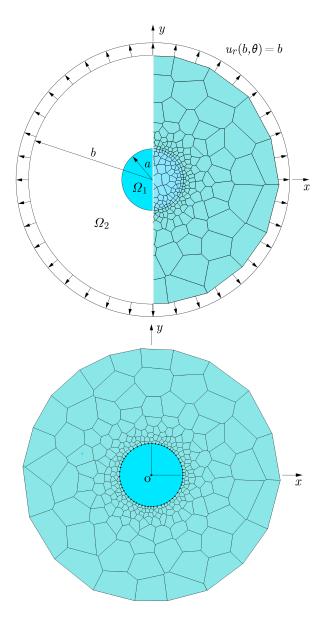
6

Figure 4: Bimaterial boundary-value problem. Model problem and boundary conditions (top left), Voronoi-cell discretization of the domain (top right) and representation of central inclusion using a single element (bottom) are shown.

due to the stiff inclusions and large-scale porosity. The corresponding results for the VCLM are quite similar, except for differences that appear along the loaded faces of the models. These differences arise from the assignment of the displacement boundary conditions (at either the Voronoi vertices or generator points for the VEM and VCLM, respectively) and the difficulties in calculating nodal stress in the VCLM along the constrained boundaries.
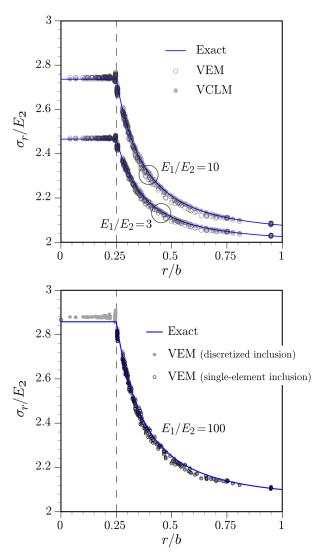

Figure 5: Radial profiles of radial stress for moderately stiff inclusions (top) and a stiff inclusion, highlighting the use of a single virtual element to represent the inclusion (bottom).

6. Conclusions

The challenges in simulating the mechanical behavior of multiphase composite materials include the effective, accurate modeling of elastic behavior, which is a determining factor for nonlinear material behavior. In this paper, we have investigated the use of the virtual element method (VEM) for modeling the deformation of such composite materials. Displacements and element stress values were compared with theory and those of Voronoi-cell lattice models (VCLM) based on the same (dual) discretization scheme. In practical terms, both the VEM and VCLM approaches provided comparably accurate results. However, the VCLM required an iterative procedure to satisfy the patch test (elastic homogeneity) for arbitrary Poisson's ratio. In addition, VCLM
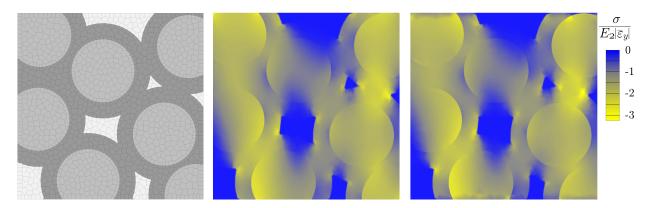
7

Figure 6: Model of macro-porous concrete under vertical compressive loading. Domain discretization (left), and contours of minor principal stress using VEM (middle) and VCLM (right) are shown.

nodes reside within the material domain, rather than on the domain boundaries, which complicates domain discretization and the assignment of boundary conditions. In this sense, the VEM has significant advantages. Furthermore, the VEM allows for stiff inclusions to each be modeled using a single polygonal element, which simplifies meshing relative to other approaches including the finite element method, particularly for irregularly shaped inclusions. A promising direction of future work is to use recent advances in the VEM on mesh-independent modeling of cracks [42] to simulate the deformation of multiphase composite materials, including cement-based composites, and their transition from continuous to discontinuous behavior.

References

[1] M. Ashby, Designing architectured materials, Scripta Materialia 68 (2013) 4–7.

[2] G. Cusatis, D. Pelessone, A. Mencarelli, Lattice discrete particle model (LDPM) for failure behavior of concrete. I: Theory, Cem Conc Compos 33 (9) (2011) 881–890.

[3] J. E. Bolander, J. Elíǎs, G. Cusatis, K. Nagai, Discrete mechanical models of concrete fracture, Eng Fract Mech 257 (2021) 108030.

[4] E. Schlangen, E. J. Garboczi, New method for simulating fracture using an elastically uniform random geometry lattice, Int J Eng Sci 34 (10) (1996) 1131–1144.

[5] L. Beirão da Veiga, F. Brezzi, A. Cangiani, G. Manzini, L. D. Marini, A. Russo, Basic principles of virtual element methods, Math Models Methods Appl Sci 23 (2013) 119–214.

[6] M. F. Benedetto, A. Caggiano, G. Etse, Virtual elements and zero thickness interface-based approach for fracture analysis of heterogeneous materials, Comput Methods Appl Mech Eng 338 (2018) 41–67.

[7] F. L. Rivarola, M. F. Benedetto, N. Labanda, G. Etse, A multiscale approach with the Virtual Element Method: Towards a VE^2 setting, Finite Elem Anal Des 158 (2019) 1–16.

[8] F. L. Rivarola, N. A. Labanda, M. F. Benedetto, G. Etse, A virtual element and interface based concurrent multiscale method for failure analysis of quasi brittle heterogeneous composites, Comput Struct 239 (2020) 106338.

[9] T. Kawai, New discrete models and their application to seismic response analysis of structures, Nuclear Eng Design 48 (1978) 207–229.

[10] J. E. Bolander, S. Saito, Fracture analyses using spring networks with random geometry, Eng Fract Mech 61 (5–6) (1998) 569–591.

[11] L. Beirão da Veiga, K. Lipnikov, G. Manzini, The Mimetic Finite Difference Method for Elliptic Problems, Vol. 11 of MS&A – Modeling, Simulation and Applications, Springer, Cham, 2014.

[12] D. P. Flanagan, T. Belytschko, A uniform strain hexahedron and quadrilateral with orthogonal hourglass control, Int J Numer Methods Eng 17 (5) (1981) 679–706.

[13] A. Cangiani, G. Manzini, A. Russo, N. Sukumar, Hourglass stabilization and the virtual element method, Int J Numer Methods Eng 102 (3–4) (2015) 404–436.

[14] K. Hormann, N. Sukumar (Eds.), Generalized Barycentric Coordinates in Computer Graphics and Computational Mechanics, Taylor & Francis, CRC Press, Boca Raton, 2017.

[15] P. Wriggers, W. T. Rust, B. D. Reddy, A virtual element method for contact, Comput Mech 58 (6) (2016) 1039–1050.

[16] A. G. Neto, B. Hudobivnik, T. F. Moherdaui, P. Wriggers, Flexible polyhedra modeled by the virtual element method in a discrete element context, Comput Methods Appl Mech Eng 387 (2021) 114163.

[17] E. Artioli, S. Marfia, E. Sacco, High-order virtual element method for the homogenization of long fiber nonlinear composites, Comput Methods Appl Mech Eng 341 (2018) 571–585.

[18] B. Ahmad, A. Alsaedi, F. Brezzi, L. D. Marini, A. Russo, Equivalent projectors for virtual element methods, Comput Math Applications 66 (2013) 376–391.

[19] L. Beirão da Veiga, F. Brezzi, L. D. Marini, A. Russo, The hitchhiker's guide to the virtual element method, Math Models Methods Appl Sci 24 (8) (2014) 1541–1573.

[20] F. Brezzi, The great beauty of VEMs, in: Proceedings of the ICM, Vol. 1, 2014, pp. 217–235.

[21] L. Beirão da Veiga, F. Dassi, A. Russo, High-order Virtual Element Method on polyhedral meshes, Comput Math Applications 74 (2017) 1110–1122.

[22] F. Dassi, L. Mascotto, Exploring high-order three dimensional virtual elements: Bases and stabilizations, Comput Math Applications 75 (9) (2018) 3379–3401.

[23] L. Beirão da Veiga, F. Brezzi, D. Marini, Virtual elements for linear elasticity problems, SIAM J Numer Anal 51 (2) (2013) 794–812.

[24] A. L. Gain, C. Talischi, G. H. Paulino, On the Virtual Element Method for three-dimensional linear elasticity problems on arbitrary polyhedral meshes, Comput Methods Appl Mech Eng 282 (2014) 132–160.

[25] E. Artioli, L. Beirão da Veiga, C. Lovadina, E. Sacco, Arbitrary order 2d virtual elements for polygonal meshes: part I, elastic problem, Comput Mech 60 (3) (2017) 355–377.

[26] H. Chi, L. Beirão da Veiga, G. H. Paulino, Some basic formulations of the virtual element method (VEM) for finite deformations, Comput Methods Appl Mech Eng 318 (2017) 148–192.

[27] P. Wriggers, B. D. Reddy, W. Rust, B. Hudobivnik, Efficient virtual element formulations for compressible and incompressible finite deformations, Comput Mech 60 (2) (2017) 253–268.

[28] M. Mengolini, M. F. Benedetto, A. M. Aragón, An engineering perspective to the virtual element method and its interplay with the standard finite element method, Comput Methods Appl Mech Eng 350 (2019) 995–1023.

[29] E. Artioli, L. Beirão Da Veiga, F. Dassi, Curvilinear virtual elements for 2D solid mechanics applications, Comput Methods Appl Mech Eng 359 (2020) 112667.

[30] N. Sukumar, M. R. Tupek, Virtual elements on agglomerated finite elements to increase the critical time step in elastodynamic simulations (2021). `arXiv:2110.00514`.

[31] M. Pingaro, E. Reccia, P. Trovalusci, R. Masiani, Fast statistical homogenization procedure (FSHP) for particle random composites using virtual element method, Comput Mech 64 (1) (2019) 197–210.

[32] M. L. Cascio, A. Milazzo, I. Benedetti, Virtual element method for computational homogenization of composite and heterogeneous materials, Compos Struct 232 (2020) 111523.

[33] A. Tabarraei, N. Sukumar, Extended finite element method on polygonal and quadtree meshes, Comput Methods Appl Mech Eng 197 (5) (2008) 425–438.

[34] K. Nagai, Y. Sato, T. Ueda, Mesoscopic simulation of failure of mortar and concrete by 3D RBSM 3 (3) (2005) 385–402.

[35] J. Eliáš, Boundary layer effect on behavior of discrete models, Materials 10 (2017) 157.

[36] J. Eliáš, Elastic properties of isotropic discrete systems: Connections between geometric structure and Poisson's ratio, Int J Solids Struct 191–192 (2020) 254–263.

[37] D. Asahina, K. Ito, J. E. Houseworth, J. T. Birkholzer, J. E. Bolander, Simulating the Poisson effect in lattice models of elastic continua, Comput Geotechnics 70 (2015) 60–67.

[38] D. Asahina, K. Aoyagi, K. Kim, J. T. Birkholzer, J. E. Bolander, Elastically-homogeneous lattice models of damage in geomaterials, Comput Geotechnics 81 (2017) 195–206.

[39] N. Sukumar, D. L. Chopp, N. Moës, T. Belytschko, Modeling holes and inclusions by level sets in the extended finite-element method, Comput Methods Appl Mech Eng 190 (2001) 6183–6200.

[40] J. Schröder, T. Wick, S. Reese, P. Wriggers, R. Müller, S. Kollmannsberger, M. Kästner, A. Schwarz, M. Igelbüscher, N. Viebahn, et al., A selection of benchmark problems in solid mechanics and applied mathematics, Arch Comput Methods Eng 28 (2) (2021) 713–751.

[41] J. P. Bardet, I. Vardoulakis, The asymmetry of stress in granular media, Int J Solids Struct 38 (2) (2001) 353–367.

[42] E. Benvenuti, A. Chiozzi, G. Manzini, N. Sukumar, Extended virtual element method for two-dimensional linear elastic fracture, Comput Methods Appl Mech Eng 380 (2022) Article 113796.